Supplement of Biogeosciences, 17, 4571–4589, 2020
https://doi.org/10.5194/bg-17-4571-2020-supplement

Biogeosciences Open Access EGU

Supplement of

Mineralization of organic matter in boreal lake sediments: rates, pathways, and nature of the fermenting substrates

François Clayer et al.

Correspondence to: François Clayer (francois.clayer@niva.no)

S1. Additional figures

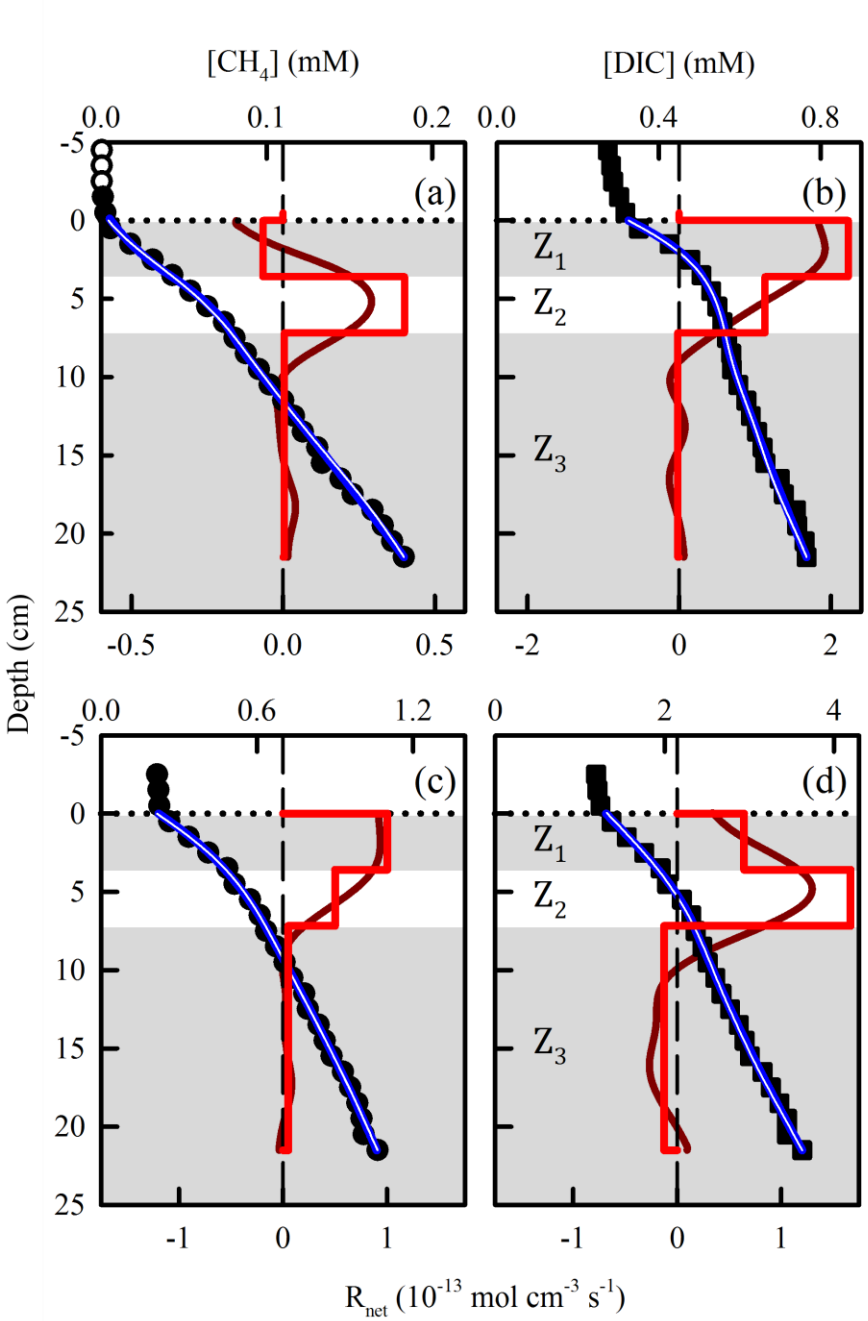

Figure S1: Comparison of concentration profiles generated with the codes PROFILE (blue line) and REC (white line) with the average (n = 3) measured concentrations (symbols) of CH_4 (a and c) and DIC (b and d) for Lake Tantaré Basin A (a and b) and Lake Bédard (c and d). The horizontal dotted line indicates the sediment-water interface. The thick red (PROFILE) and dark red (REC) lines represent the net solute reaction rate profiles.

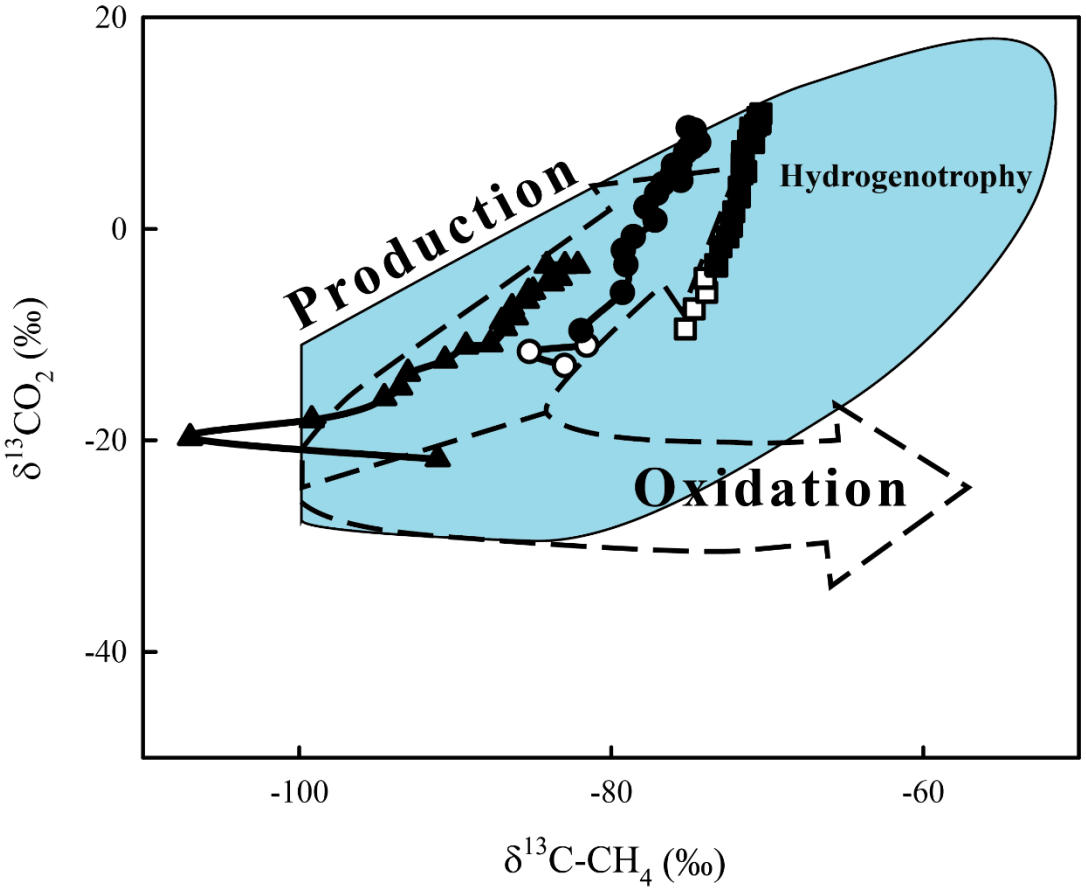

Figure S2: $\delta^{13}C$-CH_4 versus $\delta^{13}CO_2$ graph showing the hydrogenotrophy (blue) domain (modified from Whiticar 1999) along with the measured $\delta^{13}C$ data (symbols) in Lake Tantaré Basin A (triangles) and Basin B (squares; data from Clayer et al., 2018), and in Lake Bédard (circles). Empty symbols correspond to datapoints above the sediment-water interface. The $\delta^{13}C$ of gaseous CO_2 ($\delta^{13}CO_2$ on the vertical axis) was calculated from the $\delta^{13}C$-DIC according to Hélie (2004) and Mook et al. (1974).

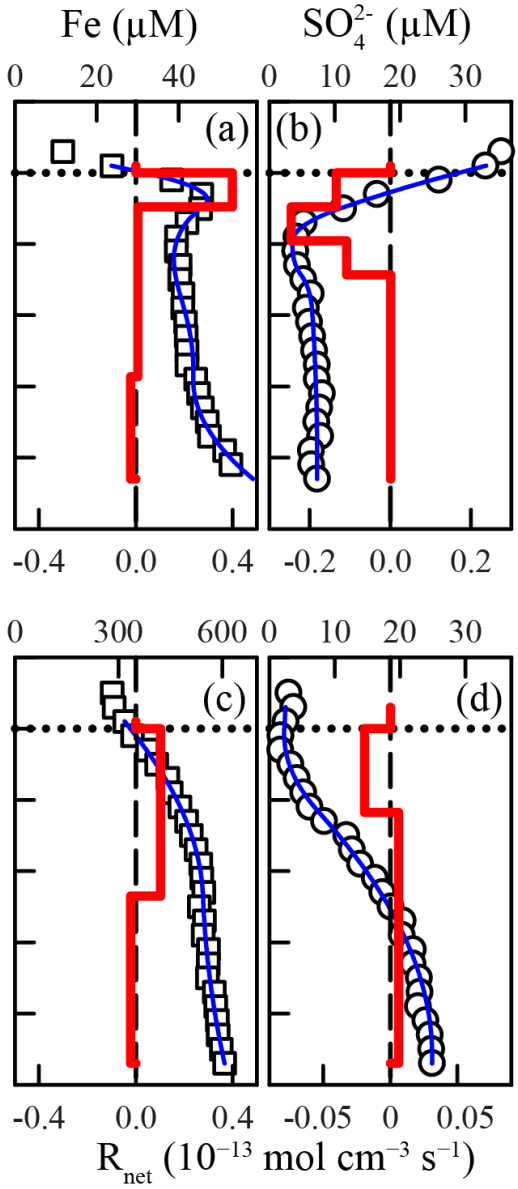

Figure S3: Comparison of the modeled (blue lines) and average (n = 3) measured (symbols) concentration profiles of SO_4 (a and c) and Fe (b and d) in Lakes Tantaré Basin A (a–b) and Bédard (c–d). The horizontal dotted line indicates the sediment-water interface. The thick red lines represent the net solute reaction rate (R_{net}^{solute}).

S2. Procedure for modeling the $\delta^{13}C$ profiles

Modeling the $\delta^{13}C$ profiles with Eq. 7, as described in section 2.4, requires first obtaining accurate [C] and [^{13}C] profiles by solving numerically, via the bvp5c function of MATLAB®, Eqs. 2 and 7 for $[C]$ and $[^{13}C]$, respectively. Equation 2 is readily solved for [C] if we use in that equation the depth distributions of $R_{net}^{CH_4}$ or R_{net}^{DIC} provided by the code PROFILE (Table 2) and those of D_s and $\alpha_{Irrigation}$, and if we impose the measured CH_4 or DIC concentrations at the top and bottom of their profiles as boundary conditions. The CH_4 and DIC profiles simulated this way are very similar to those generated by the code PROFILE, and thus to the measured distributions of these two solutes. However, extracting truthful [^{13}C] profiles from Eq. 7 is more complicated because it requires obtaining the best estimate values for the parameters f, $\delta^{13}C_i^{reactant}$, α_i, and R_i which are inherent to that equation. The approach adopted to select the best estimate values involves several steps described below.

S2.1. Simulating the $\delta^{13}C$ profiles with default parameter values in Equation 7

The first step is to perform an initial simulation of the $\delta^{13}C$ profiles using credible values (hereafter referred to as default values) for the f, $\delta^{13}C_i^{reactant}$, α_i, and R_i in Eq. 7. For the f, $\delta^{13}C_i^{reactant}$ and α_i, the default values were educated guesses based on the literature. For the rates, they were R_i values constrained with Eqs. 3–5 and the $R_{net}^{CH_4}$, R_{net}^{DIC} and R_{net}^{Ox} values provided by PROFILE (Table 2).

S2.1.1. Default values for the f, $\delta^{13}C_i^{reactant}$ and α_i

The values reported in the literature for the f-CH_4 and f-DIC as well as for the $\delta^{13}C_i^{reactant}$ and the α_i of each of the r_i outlined in Table 1, are summarized in Table S1 together with the default values. The value of f–CH_4 was estimated to be less than 1.003 (Happell et al., 1995), and that of f-DIC, lower than 1.001 (O'Leary, 1984; Jähne et al., 1987). Consequently, we chose 1.000 as the default value for both. The values of $\delta^{13}C_i^{reactant}$ used were −28‰ for OM (Joshani, 2015), and −38‰ and −18‰ for the methyl and carboxyl groups of acetate (Conrad et al., 2014), respectively, and the measured $\delta^{13}C$ values for CH_4 and DIC. We assumed no carbon fractionation during OM fermentation and oxidation, i.e., $\alpha_1 = \alpha_2 = \alpha_6 = 1.000$ (Lapham et al., 1999). Methane produced through acetoclasty (r3) and hydrogenotrophy (r4) is typically depleted in ^{13}C by 21–27‰ and 50–95‰, respectively (i.e., α_3-CH_4 and α_4 ranges are 1.021–1.027 and 1.050–1.095, respectively) compared to its substrate (Krzycki et al., 1987; Gelwicks et al., 1994; Whiticar, 1999). In addition, CO_2 and CH_4 production through acetoclasty appears to undergo similar ^{13}C depletion (Blair and Carter, 1992; Gelwicks et al., 1994). Consequently, the same intermediate fractionation factor was chosen as the default value for α_3-CH_4 and α_3-CO_2, i.e., 1.024. In agreement with Conrad et al. (2014), we used 1.075 as the default value for α_4. Several studies showed that α_5 can vary from 1.005 to 1.031 (Alperin et al., 1988; Whiticar, 1999); a default value of 1.005 was selected as in Whiticar and Faber (1986). For siderite precipitation, we calculated a composite α_7 value using the fractionation factors reported for calcite precipitation from CO_2 (0.990) or from HCO_3^- (0.998) and taking into account the relative proportion of HCO_3^- and CO_2 concentrations (Bottinga, 1969; Emrich et al., 1970).

S2.1.2. Default values for the R_i

Given that methanogenesis is dominated by hydrogenotrophy (see section 3.3), and that porewaters in all sediment zones at Lake Tantaré Basin A and in the Z_1 and Z_2 at Lake Bédard are undersaturated with respect to siderite, we assume that $R_3 = R_7 = 0$ in all the zones of the two lake basins. The only exception is for the Z_3 of Lake Bédard where we infer that siderite is precipitating (see details below). In addition, we consider that $R_2 = 0$ in all the zones of the two lake basins, except in the Z_2 of Lake Bédard where reaction r2 is required to explain the DIC net production rate (see details below). The default R_i values, obtained as described below, are reported in Table S2.

Table S1: Values of the $\delta^{13}C$ of organic matter (OM), the carboxyl group (Ac-carboxyl) and the methyl group (Ac-methyl) of acetate, and those of the molecular diffusivity ratios (f) and the isotopic fractionation factors (α_i) used as input parameters in Eq. 7.

Parameters	Range	References	Default
$\delta^{13}C$ of OM (‰ V-PDB)	−28	a	−28
$\delta^{13}C$ of Ac-carboxyl (‰ V-PDB)	−18	b, c	−18
$\delta^{13}C$ of Ac-methyl (‰ V-PDB)	−38	b, c	−38
f-DIC	1.000–1.001	d, e	1.000
f-CH_4	1.000–1.003	f	1.000
α_1, α_2 and α_6	1.000	g,h,i	1.000
α_3-CH_4	1.021–1.027	j,k,l	1.024
α_3-CO_2	1.021–1.027	k,m	1.024
α_4	1.050–1.095	l,c	1.075
α_5	1.005–1.031	l,n,o	1.005
α_7	0.990–0.998	p,q	0.995

References: (a) Joshani (2015), (b) Conrad et al (2007), (c) Conrad et al. (2014), (d) O'Leary (1984), (e) Jähne et al. (1987), (f) Happell et al., 1995, (g) Lapham et al. (1999), (h) Werth and Kusyakov (2010), (i) Conrad et al. (2012), (j) Krzycki et al. (1987), (k) Gelwicks et al. (1994), (l) Whiticar (1999), (m) Blair and Carter (1992), (n) Alperin et al. (1988), (o) Whiticar and Faber (1986), (p) Bottinga (1969), (q) Emrich et al. (1970).

S2.1.2.1. Zone of net methanotrophy

According to Fig. 2g and o, net methanotrophy is observed only in the Z_1 (0–3.6 cm) of Lake Tantaré Basin A. The net rate of DIC production in that zone (223 fmol cm^{-3} s^{-1}) is much larger than the net rate of CH_4 consumption (7 fmol cm^{-3} s^{-1}) as reported in Table 2. According to Eqs. 3 and 4, the difference between the net rates of DIC and CH_4 production is:

$$R_{net}^{DIC} - R_{net}^{CH_4} = R_1 + R_2 - 2R_4 + 2R_5 + R_6 \quad \text{(S1)}.$$

Given the large net rate of oxidant consumption ($R_{net}^{Ox} = -335$ fmol cm^{-3} s^{-1}), we assume that the contribution of R_2 in Eq. S1 can be neglected compared to that of the oxidative processes ($2R_5 + R_6$). In addition, the differences between the values of the $\delta^{13}CO_2$ and those of the $\delta^{13}C$-CH_4 (67–92‰), the large ^{13}C-CH_4 negative values (−91 to −107‰) and their upward depletion between 4.5 and 2.5 cm depth (Fig. 2b), as well as the fact that these isotopic data fall in the CO_2 reduction domain (Fig. S2), all indicate that CH_4 production by hydrogenotrophy is also active in the Z_1 of Lake Tantaré Basin A, i.e., that $R_4 \neq 0$. To simplify, we assume for now that the main oxidative process is methanotrophy and that the contribution of R_6 in Eq. S1 is negligible compared to that of $2R_5$; the effect of a possible contribution of OM oxidation to DIC will be considered in section S2.2.2.2. With the assumption that $R_2 = R_3 = R_6 = R_7 = 0$, we obtain from Eq. 3–5 the default values R_1 = 216 fmol cm^{-3} s^{-1}, R_4 = 161 fmol cm^{-3} s^{-1} and R_5 = 168 fmol cm^{-3} s^{-1}.

Table S2: Rates (R_1–R_7; fmol cm^{-3} s^{-1}) of reactions involved in OM mineralization and of siderite precipitation in each sediment zone of the two sampling sites. For each reaction rate, a default value is given and, when applicable, the range of rate values tested in modeling the $\delta^{13}C$ profiles. χ_M and χ_H are the fractions of oxidants consumed by methanotrophy and of CH_4 produced by hydrogenotrophy, respectively.

		Lake Tantaré Basin A		Lake Bédard	
Zones		Default	Range[a]	Default	Range
Z_1	R_1	216	$-105 + \chi_H(335\chi_M - 14)$	165	$-35 + 200\chi_H$
	R_2	0		0	
	R_3	0	$(1-\chi_H)\left(\frac{335}{2}\chi_M - 7\right)$	0	$100 - 100\chi_H$
	R_4	161	$\chi_H\left(\frac{335}{2}\chi_M - 7\right)$	100	$100\chi_H$
	R_5	168	$\frac{335}{2}\chi_M$	0	
	R_6	0	$335 - 335\chi_M$	0	
	R_7	0		0	
Z_2	R_1	152	$-29 + \chi_H(78 + 103\chi_M)$	100	$\frac{100COS(\chi_H - 1) - 400\chi_H}{COS - 4}$
	R_2	0		117	$117 + 100\chi_H - R_1$
	R_3	0	$(1-\chi_H)\left(39 + \frac{103}{2}\chi_M\right)$	0	$50 - 50\chi_H$
	R_4	90.5	$\chi_H\left(39 + \frac{103}{2}\chi_M\right)$	50	$50\chi_H$
	R_5	51.5	$\frac{103}{2}\chi_M$	0	
	R_6	0	$103 - 103\chi_M$	0	
	R_7	0		0	
Z_3	R_1	0		0	
	R_2	0		0	
	R_3	0		0	
	R_4	1		5	
	R_5	0		0	
	R_6	0		0	
	R_7	0		8	

[a]Note that χ_M cannot take values below 0.36 to avoid negative rate values for R_1 according to Equation S8.

S2.1.2.2. Zones of net methanogenesis

Figure 2g–h and Table 2 indicate that the value of the R_{net}^{DIC} (113 fmol cm^{-3} s^{-1}) is much larger than that of the $R_{net}^{CH_4}$ (39 fmol cm^{-3} s^{-1}) for the Z_2 of Lake Tantaré Basin A. Since oxidants are consumed at a substantial rate ($R_{net}^{Ox} = -103$ fmol cm^{-3} s^{-1}; Table 2), we conclude that DIC must be mainly produced through oxidation of CH_4 and/or OM (e.g., r5 and/or r6 in Table 1) in addition to fermentation (r1) and that R_2 can be neglected in Eq. S1. For now, we assume, as for the Z_1 of Lake Tantaré Basin A, that the only source of DIC in addition to fermentation (r1) is methanotrophy, and thus that $R_6 = 0$; the effect of a possible contribution of r6 to DIC will be considered in section S2.2.2.2. Thus, with the assumptions $R_2 = R_3 = R_6 = R_7 = 0$, we obtain from Eqs. 3–5 the default values R_1 = 152 fmol cm^{-3} s^{-1}, R_4 = 90.5 fmol cm^{-3} s^{-1} and R_5 = 51.5 fmol cm^{-3} s^{-1}.

Note that $R_1 > R_4$ does not necessarily mean that the sum of fermentation (r1) and methanogenesis via CO_2 reduction (r4) produces more DIC than CH_4 since the net rates of DIC and CH_4 production by the coupling of these two reactions are equal to $R_1 - R_4$ and R_4, respectively. For example, when glucose ($C_6H_{12}O_6$) is the fermenting substrate, the coupling of r1 and r4 produces equimolar amounts of CH_4 and DIC, i.e., $R_{net}^{CH_4} = R_{net}^{DIC}$, and the value of R_1 is then equal to twice that of R_4 ($R_1 = 2R_4$). The case when $R_1 < 2R_4$ is discussed in section 4 while the case when $R_1 > 2R_4$ is discussed below.

For the Z_1 of Lake Bédard, the $R_{net}^{CH_4}$ (100 fmol cm^{-3} s^{-1}) and the R_{net}^{DIC} (65 fmol cm^{-3} s^{-1}) are much larger than the R_{net}^{Ox} (−6.5 fmol cm^{-3} s^{-1}), suggesting that the reaction rates of the oxidative processes R_5 and R_6 can be neglected in these reduced sediments. Thus, if we assume that $R_2 = R_3 = R_5 = R_6 = R_7 = 0$, Eqs. 3 and 4 yield R_1 = 165 fmol cm^{-3} s^{-1} and R_4 = 100 fmol cm^{-3} s^{-1} as default values.

For the Z_2 of Lake Bédard, R_{net}^{Ox} (−4.5 fmol cm^{-3} s^{-1}) is much smaller than $R_{net}^{CH_4}$ (50 fmol cm^{-3} s^{-1}) and R_{net}^{DIC} (167 fmol cm^{-3} s^{-1}), indicating that, as in the Z_1, R_5 and R_6 can be neglected. With the assumptions that $R_3 = R_5 = R_6 = R_7 = 0$, we obtain from Eqs. 3 and 4 the default values $R_1 + R_2 = 217$ fmol cm^{-3} s^{-1} and $R_4 = 50$ fmol cm^{-3} s^{-1}. In this case DIC production rate is more than four times larger than R_4 ($R_{net}^{DIC} >> 2R_4$), which cannot be explained by methanogenesis alone or, given the low R_{net}^{Ox}, by oxidation reactions. Similar unanticipated DIC production has been previously attributed to the partial fermentation of HMW OM (r2, Corbett et al., 2015). Calculating individual default values for R_1 and R_2 requires an assumption about the nature of the fermenting substrate. For now, we assume that glucose is that substrate. i.e., that $R_1 = 2R_4$; the effect of considering more reduced fermenting substrates will be examined in section S2.2.2.3. With this latter assumption, the default values R_1 = 100 fmol cm^{-3} s^{-1} and R_2 = 117 fmol cm^{-3} s^{-1} are obtained.

Finally, in the Z_3 of each lake basin, the net DIC consumption rate (2 fmol cm^{-3} s^{-1} and 13 fmol cm^{-3} s^{-1}, for Lake Tantaré Basin A and Lake Bédard, respectively) and the simultaneous net CH_4 production rate (1 fmol cm^{-3} s^{-1} and 5 fmol cm^{-3} s^{-1}, for Lake Tantaré Basin A and Lake Bédard, respectively) indicate that hydrogenotrophy is active in these zones. The negative values of the R_{net}^{DIC} and the fact that the R_{net}^{Ox} = 0 suggest that the rates of the reactions producing DIC, i.e., r1, r2, r5 and r6, can be neglected. The presence of DIC in the Z_3 is likely due to its diffusion from deeper porewater (Fig. 2c and k), but not to its production in the Z_3 through the reactions listed in Table 1. Considering that $R_1 = R_2 = R_5 = R_6 = 0$, the value of R_4 is estimated with Eq. 3 to be 1 fmol cm^{-3} s^{-1} and 5 fmol cm^{-3} s^{-1}, for Lake Tantaré Basin A and Lake Bédard, respectively. Note

that in the Z_3 of Lake Bédard, the net rate value of DIC consumption exceeds by 8 fmol cm^{-3} s^{-1} that of CH_4 production suggesting that DIC is consumed by another process, in addition to hydrogenotrophy. Given that porewater is oversaturated with respect to siderite in that zone (see section 2.4) and that modeling the average Fe concentration profiles with the code PROFILE yields a net Fe consumption rate of −3 fmol cm^{-3} s^{-1} only in that zone (data not shown), we infer that siderite is precipitating at a rate of 8 fmol cm^{-3} s^{-1} in the Z_3 of Lake Bédard, i.e., R_7 = 8 fmol cm^{-3} s^{-1}.

S2.1.3. Modeled $\delta^{13}C$ profiles with the default values

The measured (symbols) $\delta^{13}C$ profiles and those simulated with the default values (purple lines) are displayed in Figure S3. A simulated profile is considered acceptable when it falls within the variability related to the sediment heterogeneity at the sampling sites (grey area fills in Fig. S3). Fig. S3a and b shows that the $\delta^{13}C$ profiles modeled with the default values do not fit adequately the datapoints in both lake basins except for the $\delta^{13}C$-CH_4 profile in Lake Bédard. These discrepancies can be due to inaccuracy of the default f and α_i and in the R_i values, a possibility that is tested below.

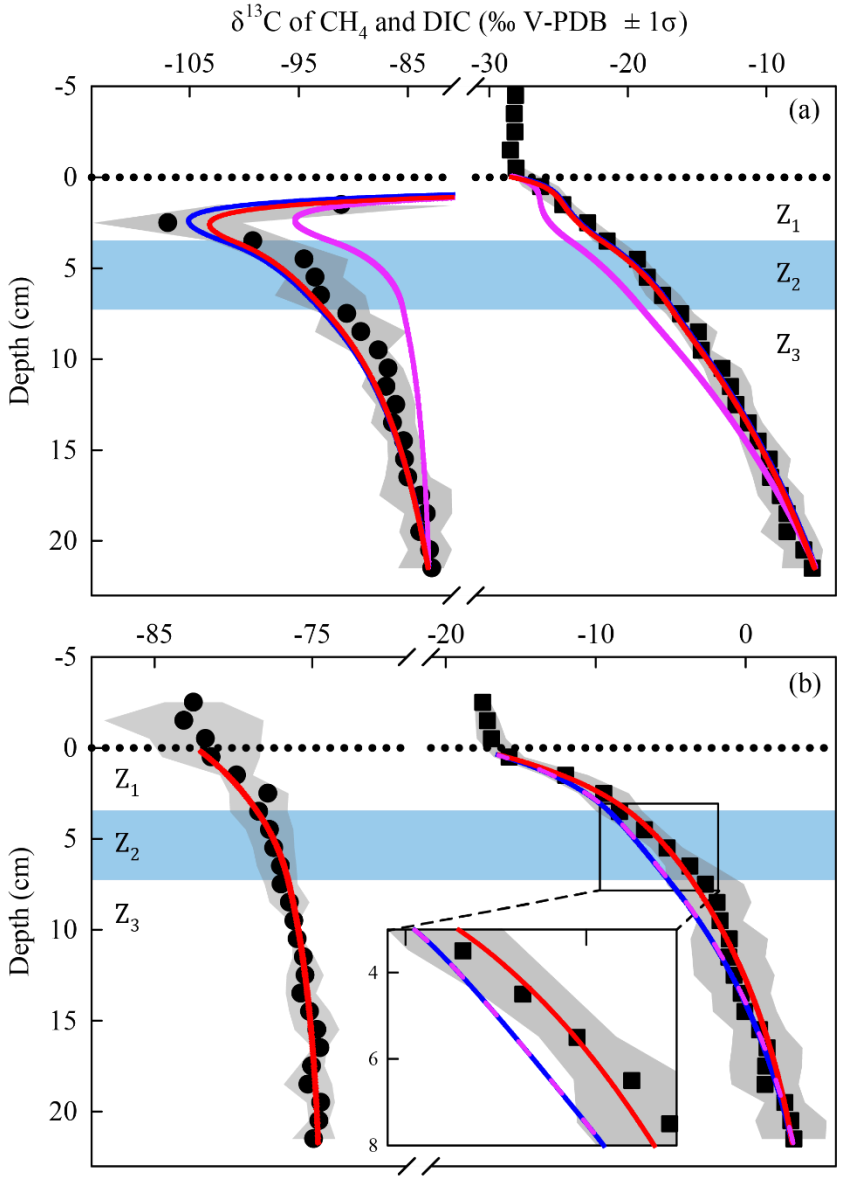

Figure S3: Comparison of the simulated (lines) and measured average (n = 3) $\delta^{13}C$ profiles of CH_4 (circles) and DIC (squares) in the porewater of Lake Tantaré Basin A (a) and Lake Bédard (b). The horizontal dotted line indicates the sediment-water interface. The variability in $\delta^{13}C$ values (± one standard deviation – σ) related to the spatial sediment heterogeneity at the sampling sites is shown by the grey area fills around the data points. The zone Z_2 is delimited by the blue area fill. The purple lines are for the profiles modeled with the default rate and parameter values displayed in tables S1 and S2, the blue lines are for the profiles simulated with the default rate values and optimal α_i and f values as described in section S2.2.1, and the red lines are for the profiles modeled with χ_M = 0.75 (panel a; see section S2.2.2.2 for details) or with α_2 values of 0.980–0.984 in the Z_2 (panel b; see section S2.2.3 for details). Note that the blue and red lines are overlapped for the $\delta^{13}C$-DIC profile in panel a and that the purple, blue and red lines are overlapped for the $\delta^{13}C$-CH_4 profile in panel b.

S2.2. Improving the fit between modeled and measured $\delta^{13}C$ profiles

S2.2.1. Optimizing the α_i and f values

Additional simulations were achieved using in Eq. 7 the default R_i values while varying α_3, α_4, α_5 and f-CH_4 within the range reported in the literature (Table S1) to improve the fits between the modeled and measured $\delta^{13}C$ profiles. Two optimization procedures, based on the minimum N_{res} values, calculated with Eq. 8 for both the $\delta^{13}C$-CH_4 and the $\delta^{13}C$-DIC profiles, were used. One, involved varying sequentially by hand first α_4 and α_3, and then the less influential parameters, i.e., α_5 and f-CH_4 (see Clayer et al., 2018 for details). The other one used a MATLAB® genetic algorithm of the global optimization toolbox, where the algorithm repeatedly provides a population of parameters within the ranges given in Table S1 to perform several hundreds of simulations. At each iteration, the genetic algorithm selects the best performing parameters from the current population and uses them as parents to produce the children parameters for the next generation. Over successive generations, the population of parameters "evolves" toward an optimal solution. The two optimization procedures yielded very similar results and thereafter, we used the MATLAB® genetic algorithm to optimize the parameters and reaction rate values. Note that, during optimization for Lake Tantaré Basin A, α_4 was allowed to take different values in the Z_1, Z_2 and Z_3.

Figure S3 shows that optimizing the f and α_i values greatly improves the fit for Lake Tantaré Basin A only and that the modeled profiles (blue lines in Fig. S3a) capture the main tendencies of the $\delta^{13}C$ profiles measured in this lake basin. Small discrepancies persist between the modeled and measured profiles (e.g., the $\delta^{13}C$-DIC profiles for Lake

Bédard) leaving the possibility that better fits could be reached if more accurate R_i values than the default values were selected.

S2.2.2. Optimizing the R_i values

Uncertainties in the R_i values may result from the assumptions that: i) all the CH_4 was produced by hydrogenotrophy in the sediments of both lake basins (sections S2.1.2.1 and S2.1.2.2), ii) OM oxidation was not a source of DIC in the Z_1 and Z_2 of Lake Tantaré Basin A (section S2.1.2.1 and S2.1.2.2), and iii) the fermenting substrate was glucose in the Z_2 of Lake Bédard (section S2.1.2.2). The mathematical expressions of the R_i have to be modified if we assume that a proportion of methanogenesis occurs via acetoclasty, that a fraction of DIC is produced through OM oxidation, or if the fermenting substrate is more reduced than glucose. The modified expressions for R_i are derived below and summarized in Table S2 for the Z_1 and Z_2 of both lake basins.

Introducing into Eq. 5, the fraction of oxidants consumed by methanotrophy (χ_M) which can take any value between 0 and 1, we can write:

$$R_5 = \frac{1}{2}\chi_M \times (-R_{net}^{Ox}) \quad \text{(S2)}$$

and:

$$R_6 = (1 - \chi_M) \times (-R_{net}^{Ox}) \quad \text{(S3)}$$

Combining Eq. 3 and S2, we obtain:

$$R_3 + R_4 = R_{net}^{CH_4} + \frac{1}{2}\chi_M \times (-R_{net}^{Ox}) \quad \text{(S4)}$$

Introducing into Eq. S4, the fraction of CH_4 produced through hydrogenotrophy (χ_H), we can write:

$$R_4 = \chi_H \left(R_{net}^{CH_4} - \frac{1}{2} \chi_M R_{net}^{Ox} \right) \quad \text{(S5)}$$

and:

$$R_3 = (1 - \chi_H) \left(R_{net}^{CH_4} - \frac{1}{2} \chi_M R_{net}^{Ox} \right) \quad \text{(S6)}$$

By combining Eqs. 3–5, and assuming that $R_7 = 0$, R_1 can be expressed:

$$R_1 = R_{net}^{DIC} - R_{net}^{CH_4} + R_{net}^{Ox} + 2R_4 - R_2 \quad \text{(S7)}$$

Combining Eqs. S5 and S7, we obtain:

$$R_1 = R_{net}^{DIC} - R_{net}^{CH_4} + R_{net}^{Ox} + \chi_H \left(2R_{net}^{CH_4} - \chi_M R_{net}^{Ox} \right) - R_2 \quad \text{(S8)}$$

The expressions for the ranges of the R_1–R_6 values displayed in Table S2, with the notable exception of R_1 in the Z_2 of Lake Bédard, were obtained by substituting into Eqs. S2, S3, S5, S6 and S8 the appropriate values of $R_{net}^{CH_4}$, R_{net}^{DIC} and R_{net}^{Ox} from Table 2. It may be recalled that in deriving these expressions, the following assumptions were made, in accordance with section S2.1.2: i) $R_2 = R_7 = 0$ in the Z_1 and Z_2 of Lake Tantaré Basin A; ii) $R_5 = R_6 = R_7 = 0$ in the Z_1 and Z_2 of Lake Bédard; iii) $R_2 = 0$ in the Z_1 , but not in the Z_2 of Lake Bédard. In order to calculate the values of R_1 with Eq. S8 for the Z_2 of Lake Bédard, we had to express R_1 as a function of the COS of the fermenting substrate as described below.

The rate of H_2 production required through r1 to sustain hydrogenotrophy is given by:

$$\left(\frac{4\nu_1 + y - 2z}{2\nu_1} \right) R_1 = 4R_4 \quad \text{(S9)}$$

Combining Eqs. S5 and S9, we obtain:

$$y = \left(\frac{2\chi_H \left(R_{net}^{CH_4} - \frac{1}{2}\chi_M R_{net}^{Ox} \right) - R_1}{R_1} \right) 4\nu_1 + 2z \quad \text{(S10)}$$

The rate of acetate production through r1 (Table 1) to sustain acetoclasty is given by:

$$\left(\frac{x - \nu_1}{2\nu_1} \right) R_1 = R_3 \quad \text{(S11)}$$

Combining Eqs. S6 and S11, we can write:

$$\nu_1 = \frac{xR_1}{2(1-\chi_H)\left(R_{net}^{CH_4} - \frac{1}{2}\chi_M R_{net}^{Ox} \right) + R_1} \quad \text{(S12)}$$

Replacing ν_1 in Eq. S10 by its expression in Eq. S12, we obtain:

$$y = \left(\frac{2R_1\chi_H \left(R_{net}^{CH_4} - \frac{1}{2}\chi_M R_{net}^{Ox} \right) - {R_1}^2}{2R_1(1-\chi_H)\left(R_{net}^{CH_4} - \frac{1}{2}\chi_M R_{net}^{Ox} \right) + {R_1}^2} \right) 4x + 2z \quad \text{(S13)}$$

The COS of an organic molecule is given by:

$$COS = -\sum_i OS_i \frac{n_i}{n_c} \quad \text{(S14)}$$

where OS_i is the oxidation state of the element *i* and n_i/n_c is its molar ratio to carbon. Assuming that the COS of the fermenting molecule is defined only by H and O atoms, whose OS are respectively +1 and −2, it can be written:

$$COS = -\left(\frac{\left[\left(\frac{2R_1\chi_H \left(R_{net}^{CH_4} - \frac{1}{2}\chi_M R_{net}^{Ox} \right) - {R_1}^2}{2R_1(1-\chi_H)\left(R_{net}^{CH_4} - \frac{1}{2}\chi_M R_{net}^{Ox} \right) + {R_1}^2} \right) 4x + 2z \right] \times (+1) + (z) \times (-2)}{x} \right) \quad \text{(S15)}$$

Eq. S15 can be simplified as:

$$R_1(2COS(1-\chi_H) + 8\chi_H)\left(R_{net}^{CH_4} - \frac{1}{2}\chi_M R_{net}^{Ox} \right) + (COS - 4){R_1}^2 = 0 \quad \text{(S16)}$$

Eq. S16 has two solutions which are $R_1 = 0$, and:

$$R_1 = \frac{(2COS(1-\chi_H) + 8\chi_H)\left(\frac{1}{2}\chi_M R_{net}^{Ox} - R_{net}^{CH_4}\right)}{COS - 4} \quad \text{(S17)}$$

The expression of R_1 for the Z_2 of Lake Bédard given in Table S2 was obtained by substituting into Eq. S17 the appropriate values of $R_{net}^{CH_4}$ and R_{net}^{Ox} from Table 2, and that of R_2 using Eq. S8.

Below, the general expressions of R_1–R_6 displayed in Table S2 for the Z_1 and Z_2 of both lake basins are used to perform additional $\delta^{13}C$ simulations and examine the effect of varying the values of χ_H, χ_M and COS on the modelled $\delta^{13}C$ profiles.

S2.2.2.1. Constraining χ_H the fraction of CH_4 produced through hydrogenotrophy

Figure S4a and b displays the N_{res} values for $\delta^{13}C$ simulations with χ_H comprised between 0.8 and 1 in the Z_1 and Z_2 of both lake basins. Note that the f and α_i values were optimized as described in section S2.2.1 for each χ_H value tested. Whereas, the N_{res} of the $\delta^{13}C$-CH_4 for Lake Tantaré Basin A and Lake Bédard does not vary with χ_H (dotted blue line in Fig. S4a and b), that of the $\delta^{13}C$ -DIC increases significantly as the value of χ_H decreases (dashed blue line in Fig. S4a and b). This finding supports our contention that the contribution of acetoclasty to methanogenesis is negligible in both lake basins, i.e., $\chi_H = 1$ (see section 3.3 and Fig. S2).

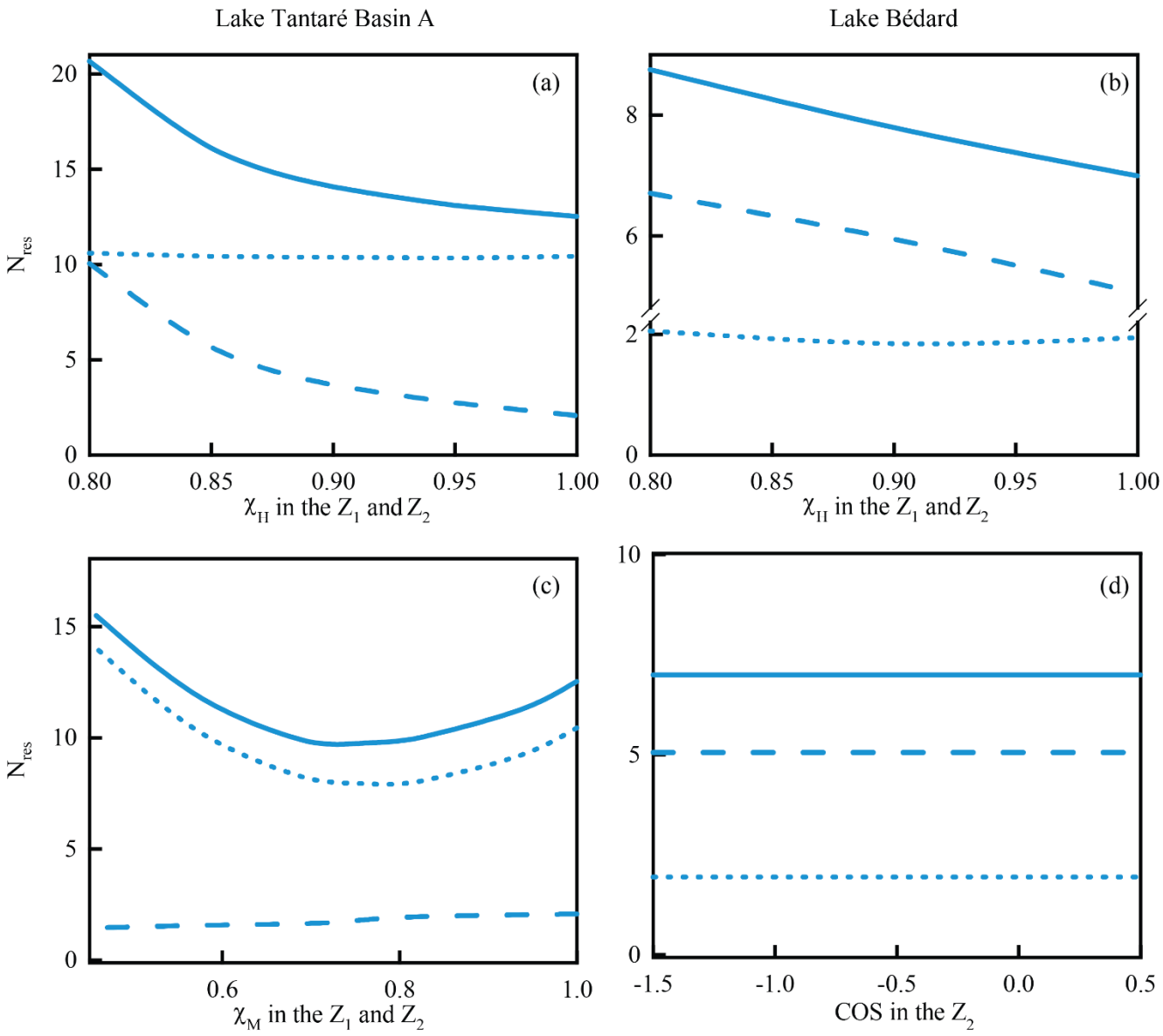

Figure S4: Norm of residuals (N_{res}), calculated with Eq. (8), for the δ^{13}C-DIC (dashed line) and the δ^{13}C-CH_4 (dotted line) profiles, and the sum of N_{res} for the two profiles (solid lines). In panels a and b, the N_{res} values are displayed as a function of χ_H for the Z_1 and Z_2 of both lake basins, in panel c, as a function of χ_M for the Z_1 and Z_2 of Lake Tantaré Basin A, and in panel d, as a function of the COS for the Z_2 of Lake Bédard.

S2.2.2.2. Constraining χ_M the fraction of oxidant consumed through methanotrophy

In section S2.1.2.2, we neglected OM oxidation as a source of DIC in the Z_1 and Z_2 of Lake Tantaré Basin A. Figure S4c shows that the sum of N_{res} for the $\delta^{13}C$-CH_4 and the $\delta^{13}C$-DIC profile displays a minimum at a χ_M value of about 0.75, when χ_M is varied between 0.36 and 1, while maintaining χ_H at 1 and optimizing the f and α_i as in section S2.2.1. Fig S3a (red line) shows that using χ_M = 0.75 in the simulation results in a slightly improved fit of the $\delta^{13}C$-CH_4 profile. This χ_M value implies that about 25% of the oxidant are consumed through OM oxidation in the Z_1 and Z_2 of Lake Tantaré Basin A. Assuming that χ_M = 0.75, we calculate with the equations reported in Table S2 that: R_1 = 132 fmol cm^{-3} s^{-1}, R_4 = 119 fmol cm^{-3} s^{-1}, R_5 = 126 fmol cm^{-3} s^{-1} and R_6 = 84 fmol cm^{-3} s^{-1} in the Z_1 and R_1 = 126 fmol cm^{-3} s^{-1}, R_4 = 78 fmol cm^{-3} s^{-1}, R_5 = 39 fmol cm^{-3} s^{-1} and R_6 = 26 fmol cm^{-3} s^{-1} in the Z_2 (Table 3).

S2.2.2.3. Influence of the COS in the Z_2 of Lake Bédard

Figure S4d shows that varying the value of the COS between −1.5 and +0.5, while maintaining χ_H at 1 and optimizing the f and α_i as in section S2.2.1 has no influence on the modelled $\delta^{13}C$ profiles, i.e., it yields similar N_{res} values. This result was expected given that the COS only affects the values of R_1 and R_2 and that we assumed no fractionation for reactions r1 and r2, as generally proposed in the literature (Lapham et al., 1999; Werth and Kusyakov, 2010; Conrad et al., 2012; Corbet et al., 2015). However, Fig. S3b exhibits a discrepancy between the measured and modeled $\delta^{13}C$-DIC profiles of Lake Bédard. To test if an isotopic fractionation of the DIC assumed to be produced by partial fermentation of HMW OM in the Z_2 of lake Bédard, could explain this discrepancy, we varied α_2 in the simulations. Figure S5 reveals that a minimum N_{res} is

obtained at a value of α_2 = 0.980 for a COS value of 0, as assumed in section S2.1.2.2, and Fig. S3b (red line) shows that using this α_2 value in the simulation results in an improved fit of the δ^{13}C-DIC profile for Lake Bédard. The optimum α_2 value vary slightly with the COS value inferred. For example, for a COS value of −1.5, the optimum α_2 value would be 0.984 (Fig. S5). Varying the COS within reasonable values, however, does not influence significantly the fitting of the δ^{13}C-DIC profile for Lake Bédard shown by the red line in Fig. S3d. Assuming that the COS = −1.5 in the Z_2 of Lake Bédard, we calculate with the equations reported in Table S2 that: R_1 = 72 fmol cm^{-3} s^{-1}, R_2 = 145 fmol cm^{-3} s^{-1} and R_4 = 50 fmol cm^{-3} s^{-1} (Table 3). Note that, considering an α_2 value between 0.980 and 0.984 for the DIC produced through reaction r2 and a δ^{13}C signature of −28‰ for the HMW OM is equivalent to assuming no isotopic fractionation (i.e., α_2 = 0) and a δ^{13}C signature of −8‰ to −12‰ for the source material.

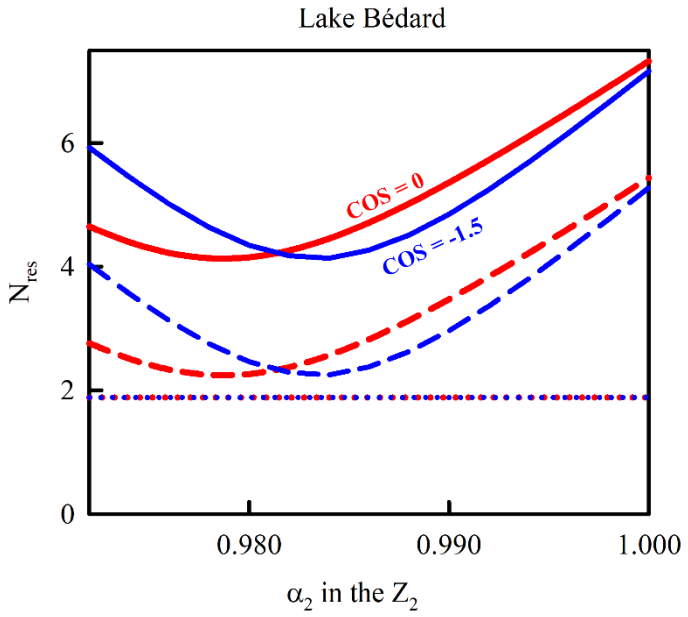

Figure S5: Norm of residuals (N_{res}), calculated with Eq. (8), for the simulated δ^{13}C-DIC (dashed line) and the δ^{13}C-CH_4 (dotted line) profiles, and the sum of N_{res} for the two profiles (solid line) as a function of the value of α_2 in the Z_2 of Lake Bédard.

S3. Other data from Lakes Tantaré, Bédard, Jacks and Lugano used to calculate the COS.

S3.1. Relevant data available and lake characteristics.

Porewater profiles of solutes relevant to the COS calculation, measured by our group in Lakes Tantaré and Bédard at other dates than in the present study, are available from our earlier publications or from our data repository. Profiles of porewater CH_4, DIC, SO_4^{2-}, sulfides (ΣS(−II)) and Fe, determined at the deepest site in the perennially oxic Basin A of Lake Tantaré in September 2004, October 2005, September 2006 and July 2012, have been reported by Clayer et al. (2016). Vertical profiles of the same solutes measured at the deepest site in the sediments of Basin B of Lake Tantaré in October 2006, July 2007, October 2011 and October 2014 can also be found in Clayer et al. (2016 and 2018); the $\delta^{13}C$ profiles of CH_4 and DIC are also provided for the October 2014 campaign (Clayer et al. 2018). Basins A and B of Lake Tantaré, the two westernmost basins of Lake Tantaré, are connected by a shallow channel. This lake is oligotrophic, with a planktonic primary production of 50 mg C m^{-2} d^{-1} measured in Basin A (Hare et al. 1994). Bottom water in Basin B, in contrast to that of Basin A, becomes occasionally anoxic in late summer (Couture et al., 2008). Also, its ^{210}Pb profile reveals no mixing in the uppermost sediment layers and the ^{137}Cs, ^{241}Am and mid-19th century Upper Mississippi Valley Pb isotope chronostratigraphic markers, all display sharp peaks (Gobeil et al., 2013). Collectively, these observations indicate that benthic invertebrates are virtually absent at that site and that solute transport across the sediment-water interface (SWI) should be by molecular diffusion alone. Couture et al. (2010) provide porewater SO_4^{2-}, ΣS(−II)), and Fe profiles determined in June 2004 at the deepest site in

Lake Bédard, and an unpublished set of porewater profiles of CH_4, DIC, SO_4^{2-}, ΣS(−II) and Fe obtained in October 2003 by our group with the methods described by Clayer et al. (2016) is also available from our archives. The profiles of ^{210}Pb, ^{137}Cs, and stable Pb isotope (Gobeil et al., 2013) all point out to the absence of benthic invertebrates in Lake Bédard sediments.

Carignan and Lean (1991) reported porewater DIC, CH_4, NH_4, ΣS(−II), P, Si, Fe, Mn, Ca, Mg, K and pH profiles obtained in September 1981 with peepers at 5 sites of varying depth (4, 10, 15, 20.2 and 21.7 m) along a transect in the Williams Bay of Jacks Lake (44º41' N, 78º02' W). This lake is located ~65 km north of Peterborough, Ontario, on the fringe of the Canadian Shield and the bedrock of its forested watershed comprises mainly felsic rocks with minor limestone outcroppings (Pick et al., 1984). The dimictic Williams Bay is mesotrophic, with a ^{14}C primary production of ~900 mg C m^{-2} d^{-1}, and it develops an anoxic hypolimnion from mid-June to September. The presence of ΣS(−II) in the water overlying the sediments indicates anoxia at the sediment surface of all stations in September. Carignan and Lean (1991) mention that macrobenthos activity at the two shallowest stations should be suspected from the ^{210}Pb and the DIC and CH_4 profiles, and that a loss of CH_4 may have occurred during retrieval and sampling of the peepers and have altered the lower part (below ~30 cm) of the CH_4 profiles at the three deepest stations. The authors identified by SEM/EDAX solid Fe sulfide particles ($FeS_{2(s)}$ and $FeS_{(s)}$) in the sediments of the three deepest stations but were unable to detect carbonates ($FeCO_{3(s)}$ or $CaCO_{3(s)}$).

Porewater profiles of CH_4, DIC, Ca, Fe, SO_4^{2-} and ΣS(−II) have been obtained with peepers (Lazzaretti et al., 1992; Lazzaretti-Ulmer and Hanselmann, 1999) in June

1989, September 1989 and March 1990 at two sites (Melide, 85 m depth and Figino, 95 m depth) located in the southern basin of Lake Lugano (46°00'N; 03°30'E; Switzerland). This lake basin is monomictic, with the overturn occurring in February. It was originally oligotrophic but it had become eutrophic in 1989 for more than 30 years due to increasing nutrient loads, and it showed a primary production rate of up to ~1260 mg C m^{-2} d^{-1} (Barberi and Mosello, 1992; Niessen et al., 1992). As shown in the papers by Lazzaretti et al. (1992) and Lazzaretti-Ulmer and Hanselmann (1999), the redox conditions at the SWI varied markedly with time. In the overlying water, in March 1990, [O_2] concentration was ~2 and 4 mg L^{-1} at the Figino and Melide sites, respectively, and ΣS(−II), CH_4, Fe(II) and Mn(II) were absent in the lake bottom water, supporting oxidizing conditions at the SWI at the two sites at that date. In contrast, in June and September 1989, the SWI at the two sites was anoxic since ΣS(−II), CH_4, Fe(II) and Mn(II) were present in the overlying water (except Fe in June at the Figino site). The sediments at the two sites are characterized by the presence of carbonate and clay varves (Span et al., 1992) and by the absence of benthos remains in the pre-1970 layers (Niessen et al., 1992), indicating the absence on benthic animals.

S.3.2. Data treatment

The relevant porewater profiles for Lake Bédard and for the two basins of Lake Tantaré were gathered from our archives or from our earlier publications. For Williams Bay of Jacks Lake and for Lake Lugano, the published plots of the porewater solutes of interest were enlarged electronically, and the coordinates of the data points were determined to reconstruct the solute concentration vs depth profiles. The measured CH_4 and DIC profiles for Lakes Tantaré, Bédard, Jacks (Williams Bay) and Lugano along

with their respective modeled profiles using the code PROFILE are displayed in Fig. 4. For Williams Bay, only the profiles reported at 15 m and 22 m were retained in this study; those from the two shallowest sites (4 m and 10 m) were ignored because of sediment bioirrigation (Carignan and Lean 1991), whereas those from the 20-m site were discarded because modeling with PROFILE predicted an extremely low net DIC production rate. For Lake Lugano, the data pertaining to March 1990 and June 1989 were kept; those reported for September 1989 were rejected because the CH_4 and DIC concentration profiles were almost linear and modeling with PROFILE did not show any zone of significant net CH_4 production. The R_{net}^{Ox} values were calculated, as described in section 2.3, from the consumption rates of the electron acceptors (EAs; O_2, Mn(IV), Fe(III) and SO_4^{2-}) obtained by modeling the porewater depth distributions of O_2, Mn(II), Fe(II) and SO_4^{2-} with the code PROFILE. To estimate the contribution of the O_2 consumption rate to R_{net}^{Ox} in March at the two sites of Lake Lugano, we assumed that the $[O_2]$ at the sediment surface was 2 $mg.L^{-1}$ at Figino and 4 $mg.L^{-1}$ at Mélide, i.e., the concentrations measured in the water column, near the sediment surface at these sites (Lazzaretti et al, 1992). The absence of sulfate data for Williams Bay prevented us from calculating R_{net}^{Ox}. The production rate of DIC due to carbonate dissolution in the porewaters was calculated by modeling with PROFILE the porewater Ca profiles for the two sites in Lake Lugano, and its contribution was removed from the R_{net}^{DIC}; this calculation was unnecessary for Williams Bay where this dissolution reaction did not occur. In modeling with PROFILE, we assumed that $\alpha_{irrigation}$ was negligible, even in March for the two sites at Lake Lugano, given the evidence that macrobenthos is absent. Note that the R_{net}^{DIC} and R_{net}^{Ox}values are weighed average values calculated over a zone of net methanogenesis. The $R_{net}^{CH_4}$, R_{net}^{DIC} and R_{net}^{Ox} values are regrouped in Table 4 for the various lake basins.

References

Alperin M.J., Reeburgh W.S. and Whiticar M.J. (1988) Carbon and hydrogen isotope fraction resulting from anaerobic methane oxidation. Global Biogeochem. Cycles 2**:** 279-288.

Barberi A. and Mosello R. (1992) Chemistry and trophic evolution of Lake Lugano in relation to nutrient budget. Aquatic Sci. 54: 219-237.

Blair N.E. and Carter J.W.D. (1992) The carbon isotope biogeochemistry of acetate from a methanogenic marine sediment. Geochim. Cosmochim. Acta 56**:** 1247-1258.

Bottinga Y. (1969) Calculated fractionation factors for carbon and hydrogen isotope exchange in the system calcite-carbon dioxide-graphite-methane-hydrogen-water vapor. Geochim. Cosmochim. Acta 33**:** 49-64.

Carignan R. and Lean D.R.S. (1991) Regeneration of dissolved substances in a seasonally anoxic lake: the relative importance of processes occurring in the water column and in the sediments. Limnol. Oceanogr. 36: 683-707.

Clayer F., Gobeil C. and Tessier A. (2016) Rates and pathways of sedimentary organic matter mineralization in two basins of a boreal lake: emphasis on methanogenesis and methanotrophy. Limnol. Oceanogr. 61: S131-S149.

Clayer F., Moritz A., Gélinas Y., Tessier A. and Gobeil C. (2018) Modeling the carbon isotope signatures of methane and dissolved inorganic carbon to unravel mineralization pathways in boreal lake sediments. Geochim. Cosmochim. Acta 229**:** 36-52.

Conrad R., Chan O.C., Claus P. and Casper P. (2007) Characterization of methanogenic Archaea and stable isotope fractionation during methane production in the profundal sediment of an oligotrophic lake (Lake Stechlin, Germany). Limnol. Oceanogr. 52**:** 1393-1406.

Conrad R., Klose M., Yuan Q., Lu Y. and Chidthaisong A. (2012) Stable carbon isotope fractionation, carbon flux partitioning and priming effects in anoxic soils during methanogenic degradation of straw and soil organic matter. Soil Biol. Biochem. 49**:** 193-199.

Conrad R., Claus P., Chidthaisong A., Lu Y., Fernandez Scavino A., Liu Y., Angel R., Galand P.E., Casper P., Guerin F. and Enrich-Prast A. (2014) Stable carbon isotope biogeochemistry of propionate and acetate in methanogenic soils and lake sediments. Org. Geochem. 73**:** 1-7.

Corbett J.E., Tfaily M.M., Burdige D.J., Glaser P.H. and Chanton J.P. (2015) The relative importance of methanogenesis in the decomposition of organic matter in northern peatlands. J. Geophys. Res.: Biogeosci. 120**:** 280-293.

Couture R.-M., Gobeil C. and Tessier A. (2008) Chronology of atmospheric deposition of arsenic inferred from reconstructed sedimentary records. Environ. Sci. Technol. 42: 6508-6513.

Couture R.-M., Gobeil C. and Tessier A. (2010) Arsenic, iron and sulfur co-diagenesis in lake sediments. Geochim. Cosmochim. Acta 74: 1238-1255.

Emrich K., Ehhalt D.H. and Vogel J.C. (1970) Carbon isotope fractionation during the precipitation of calcium carbonate. Earth. Planet. Sci. Lett. 8**:** 363-371.

Gelwicks J.T., Risatti J.B. and Hayes J.M. (1994) Carbon isotope effects associated with aceticlastic methanogenesis. Appl Environ Microbiol 60**:** 467-472.

Gobeil C., Tessier A. and Couture, R.-M. (2013) Upper Mississippi Pb as a mid-1800s chronostratigraphic marker in sediments from seasonally anoxic lakes in Eastern Canada. Geochim. Cosmochim. Acta 113: 125-135.

Happell J.D., Chanton J.P. and Showers W.J. (1995) Methane transfer across the water-air interface in stagnant wooded swamps of Florida: Evaluation of mass-transfer coefficients and isotopic fractionation. Limnol. Oceanogr. 40**:** 290-298.

Hare L., Carignan R. and M. A. Huerta-Diaz (1994) A field study of metal toxicity and accumulation by benthic invertebrates; implications for the acid-volatile sulfide (AVS) model. Limnol. Oceanogr. 39: 1653-1668.

Hélie J.-F. (2004) Géochimie et flux de carbone organique et inorganique dans les milieux aquatiques de l'est du Canada : exemples du Saint-Laurent et du réservoir Robert-Bourassa -approche isotopique -. Ph.D. thesis, Université du Québec à Montréal.

Jähne B., Heinz G. and Dietrich W. (1987) Measurement of the diffusion coefficients of sparingly soluble gases in water. J. Geophys. Res. 92**:** 10767-10776.

Joshani A. (2015) Investigating organic matter preservation through complexation with iron oxides in Lake Tantaré. M.Sc. thesis, Concordia University.

Krzycki J.A., Kenealy W.R., DeNiro M.J. and Zeikus J.G. (1987) Stable carbon isotope fractionation by *Methanosarcina barkeri* during methanogenesis from acetate, methanol, or carbon dioxide-hydrogen. Appl Environ Microbiol 53**:** 2597-2599.

Lapham L., Proctor L. and Chanton J. (1999) Using respiration rates and stable carbon isotopes to monitor the biodegradation of orimulsion by marine benthic bacteria. Environ. Sci. Technol. 33**:** 2035-2039.

Lazzaretti M.A., Hanselmann K.W., Brandl H., Span D. and Bachofen R. (1992) The role of sediments in the phosphorus cycle in Lake Lugano. II. Seasonal and spatial variability of microbiological processes at the sediment-water interface. Aquatic Sci. 54: 285-299.

Lazzaretti-Ulmer M.A. and Hanselmann K.W. (1999) Seasonal variation of the microbially regulated buffering capacity at sediment-water interfaces in a freshwater lake. Aquatic Sci. 61: 50-74.

Mook W. G., Bommerson J. C. and Staverman W. H. (1974) Carbon isotope fractionation between dissolved bicarbonate and gaseous carbon dioxide. Earth Planet. Sci. Lett. 22**:** 169-176.

Niessen F., Wick L., Bonani G., Chondrogianni C. and Siegenthaler C. (1992) Aquatic system response to climatic and human changes: productivity, bottom water oxygen status, and sapropel formation in Lake Lugano over the last 10 000 years. Aquatic Sci. 54: 257-276.

O'Leary M.H. (1984) Measurement of the isotope fractionation associated with diffusion of carbon dioxide in aqueous solution. J. Phys. Chem. 88**:** 823-825.

Pick F.R., Lean D.R.S. and Nalewajko C. (1984) Nutrient status of metalimnetic phytoplankton peaks. Limnol. Oceanogr. 29: 960-971.

Span D., Dominik J., Lazzaretti M.A. and Vernet J.-P. (1992) The role of sediments in the phosphorus cycle in Lake Lugano. I. Geochemical approach. Aquatic Sci. 54: 277-284.

Werth M. and Kuzyakov Y. (2010) ^{13}C fractionation at the root–microorganisms–soil interface: A review and outlook for partitioning studies. Soil Biol. Biochem. 42**:** 1372-1384.

Whiticar M.J. (1999) Carbon and hydrogen isotope systematics of bacterial formation and oxidation of methane. Chem. Geol. 161**:** 291-314.

Whiticar M.J. and Faber E. (1986) Methane oxidation in sediment and water column environments—Isotope evidence. Org. Geochem. 10**:** 759-768.